Improved Limits on $n \to n'$ Transitions from the Spallation Neutron Source

Francisco M. Gonzalez,[1] Leah J. Broussard,[1] Lisa DeBeer-Schmitt,[1] Michael R. Fitzsimmons,[1] Matthew J. Frost,[1] Lawrence Heilbronn,[2] Erik B. Iverson,[1] Yuri Kamyshkov,[2] Michael Kline,[3] and TODO: Fill out rest of author list[4]

[1]*Oak Ridge National Laboratory, Oak Ridge, TN 37831, USA*
[2]*University of Tennessee, Knoxville, TN 37996, USA*
[3]*Department of Physics, The Ohio State University, Columbus, OH 43210, USA*
[4]*See TODO*

(Dated: Whenever we finish analysis)

A proposed mechanism of Baryon Number $\mathcal{B}$ violation, neutrons oscillating into their right-handed mirror companions, is studied. We present upon updated limits of a particular type of this model, wherein a small but non-zero mass difference exists between the neutron and its mirror state. We do a search for this.

INTRODUCTION

Motivation

Much of the matter in the universe is invisible, not interacting via the electromagnetic force. This "dark matter" has thus far evaded direct detection, which has led to a robust suite of experimental and theoretical proposals looking for new exotic particles and interactions [1, 2]. The traditional Cold Dark Matter (CDM) paradigm, featuring non-relativistic matter interacting only by gravity, stands in tension with the observations of the density profiles of the dark matter halos of galaxies. One possible solution to this cusp/core problem introduces new forces acting between dark matter particles within a model of Self-Interacting Dark Matter [3, 4]. Theories of Self-Interacting Dark Matter vary in complexity from introduction of exotic forces all the way up to atomic Dark Matter [5].

At the opposite end of the size spectrum from galaxies, the Weak interaction in the Standard Model (SM) of particle physics is left-handed and maximally breaks parity. Early attempts to resolve this apparent fine-tuning posited a right-handed equivalent of the Weak interaction and subsequently right-handed copies of the SM [6, 7]. This right-handed Mirror Model would completely duplicate the $SU(3) \times SU(2) \times U(1)$ form of the SM with a dark sector denoted $SU'(3) \times SU'(2) \times U'(1)$ [8**?**].

The Mirror Model would interact with normal matter predominately through gravity, making it a candidate for a type of Self-Interacting Dark Matter. Mirror Matter, having the same interactions as the standard model, could have similar complexity to Standard Model matter on cosmological scales [9]. The added particles and forces would have implications for element formation in the early universe, and could even be a mechanism for a non-zero cosmological constant [10, 11]. This could potentially lead to the formation of Mirror Matter based"Dark Stars," or mixed stars with a dark matter subcomponent [12, 13]. Such exotic objects could be searched for with existing astrophysical dark matter searches, in conjunction with laboratory searches for dark matter's underlying particle nature [14].

Leah: A little background on NNBAR

One of the major unsolved questions in physics is the universe's matter-antimatter asymmetry, which requires a violation of Baryon number $\mathcal{B}$ or Lepton number $\mathcal{L}$. In a universe with Mirror Matter, Standard Model neutral particles such as the neutron, n, or neutrinos, ν, could mix with their Mirror counterparts. Such mixing would cause $\mathcal{B}$ violation in the neutron sector or $\mathcal{L}$ violation in the neutrino sector. The neutron, due to its relatively long lifetime and relative ease of trapping, would be a natural candidate for studying Mirror Matter in the laboratory. Neutrons would oscillate into their mirror counterpart n', with some characteristic mixing mass denoted as $\epsilon_{nn'}$. This mixing can be contrasted with the more well-studied neutron-antineutron $n \to \bar{n}$ oscillations, as a $\Delta\mathcal{B} = 1$ process, rather than the $\Delta\mathcal{B} = 2$ for $n \to \bar{n}$ [15, 16]. Mirror neutrons could be an intermediary process to $n \to \bar{n}$ conversion, $n \to n' \to \bar{n}$, which would have significantly reduced limits [17].

Outside of the explicit Mirror Model, a potential sterile partner of the neutron n' has been proposed as a probe of multiple branes [18].

Yuri: STEREO thing about QFT vs. gravity. Also Pospelov(?) criticism

Mirror Matter Phenomenology

In this model, the neutron n is mixed with its dark partner from the mirror sector, a sterile "mirror" neutron n'.

Yuri: More history on the phenomenology

The theoretical model probed in this paper was originally proposed in [19] as a potential explanation for the "neutron lifetime anomaly." The lifetime of ultracold neutrons (UCN) stored inside of a magnetic or material "bottle" has been measured as $\tau_n = 878.4 \pm 0.5$ [20–27]. This value disagrees with the lifetime of $\tau_n = 888.0 \pm 0.7$ s determined by measuring neutron decay products in a cold neutron “beam” by $> 4\sigma$ [28–30]. The paper [19] hypothesizes that the increase of $\sim 1\%$ in the measured τ_n as the result of an increased $n \to n'$ oscillation probability due to the magnetic fields $\vec{B}$ present in the most precise “beam” experiment [28, 29].

A neutron traveling through a magnetic field $\vec{B}$ and material with optical potential $V - iW$, where $V > 0$ is the real part of the potential and W is the corresponding imaginary part, has a Hamiltonian given by [31]:

$$\mathcal{H}_n = m_n + \frac{p_n^2}{2m_n} + \mu_n \vec{\sigma} \cdot \vec{B} + V - i\left(W + \frac{\Gamma}{2}\right) \quad (1)$$

In equation 1 the intrinsic properties of the neutron, m_n and μ_n, refer to the mass and magnetic moment respectively, and we work in natural units such that $c = 1$. The vector of Pauli matrices that describes the neutron's spin is represented as $\vec{\sigma}$. The imaginary component of the Hamiltonian coming from the Fermi potential W and the neutron decay rate Γ describe neutron loss mechanisms.

The Z_2 symmetry between ordinary and mirror sectors can be spontaneously broken either at a high-energy scale or due to limited-range new forces. Such a difference in the Higgs vacuum expectation value would induce a small mass splitting $\Delta m = m_n \pm m_{n'}$ between the n and n'. The variation in masses is unknown and as such the neutron mass, m_n, can be either greater than or less than its mirror counterpart's mass, $m_{n'}$. This mass difference works to suppress the probability of $n \to n'$ oscillations for free neutrons in the absence of strong magnetic fields. Equation 1 can be extended to the mirror sector, with a mass and magnetic dipole moment that could differ due to a difference in the Higgs vacuum expectation value:

$$\mathcal{H}_{n'} = m_{n'} + \frac{p_{n'}^2}{2m_{n'}} + \mu_{n'} \vec{\sigma} \cdot \vec{B}' + V' - i\left(W' + \frac{\Gamma'}{2}\right) \quad (2)$$

Evolution of (n, n') system follows the Schrödinger equation $id\Psi/dt = H\Psi$, where Ψ is the wavefunction of n and n' components in two ($\pm$) spin polarization states $\Psi = (\psi_n^+, \psi_n^-, \psi_{n'}^+, \psi_{n'}^-)^T$. The evolution of the two-state (n, n') system can then be described introducing an unknown mixing parameter $\epsilon_{nn'}$ in the 4×4 Hamiltonian for such a Schrödinger equation:

$$\frac{d}{dt}\Psi = \begin{pmatrix} \mathcal{H}_n & \epsilon_{nn'} \\ \epsilon_{nn'} & \mathcal{H}_{n'} \end{pmatrix} \Psi \quad (3)$$

In the most general case, the transition element $\epsilon_{nn'}$ can contain a transition magnetic moment $\vec{\eta}_B$ or electric $\vec{\eta}_E$ moment, which could couple to the respective standard and mirror fields and cause a transition magnetic or electric moment [32]. The search described in this paper assumes that such couplings $\vec{\eta}_B$ and $\vec{\eta}_E$ are zero.[1]

Although equation 3 generically describes the (n, n') system, some simplifying assumptions will be made. Due to conservation of momentum, the difference in the $\frac{p_n^2}{2m_n}$ terms will be negligible. A difference in the magnitude of the magnetic dipole moments μ_n between neutrons and their mirror partners would appear the same as a difference in the magnitude of the unobserved quantity $\vec{B}'$, and so the magnetic dipole moments can be assumed to be identical. The magnetic field in the laboratory B interacts only with the magnetic moment of the neutron, μ_n and not with the magnetic moment of the mirror neutron, $\mu_{n'}$. Although a large mirror magnetic field $\vec{B}'$ in free space can not be ruled out, the dark matter density of Earth suggests the mirror material potentials V' and W' to be vanishing [33]. Since the time of flight of cold neutrons ($\mathcal{O}(ms)$) is significantly less than the neutron lifetime ($\tau_n \approx 880$ s), the decay rates Γ and Γ' are taken to be negligible. As a result, we can use the simplified 4×4 matrix Hamiltonian:

$$\mathcal{H} = \begin{pmatrix} m_n + \mu_n \vec{\sigma} \cdot \vec{B} + V - iW & \epsilon_{nn'} \\ \epsilon_{nn'} & m_n \pm \Delta m \end{pmatrix} \quad (4)$$

This interaction Hamiltonian induces an oscillation in $n \to n'$, which can then be tuned by changes in the magnetic fields, material potentials, and fundamental properties of the n and n'. The mass difference Δm serves to suppress the oscillation probability of free neutrons outside of strong magnetic fields or exactly compensating material potentials. The oscillation probability must be less than $\sim 10^{-6}$ in order to satisfy requirements of neutron storage inside of material traps [20, 23, 25]. For a mass difference $\Delta m \sim 100$ neV, the oscillation length for neutrons inside a trap is shorter than a micron. In this case, the average probability during a collision with the wall is half the square of the maximum amplitude of oscillation. Such an effect would thus lead to a measurable loss rate of $n \to n'$ as a function of free flight time inside of the material trap.

In vacuum, and in the absence of magnetic field B, the probability of $n \to n'$ transformation becomes [19]:

$$P_{nn'} = 1 - P_{nn} = \frac{1}{2}\sin^2 2\theta_0 \simeq 2\theta_0^2 = 2\left(\frac{\epsilon_{nn'}}{\Delta m}\right)^2 \quad (5)$$

Equation 5 introduces the mixing angle $\tan 2\theta_0 \equiv 2\epsilon_{nn'}/\Delta m$ which we use as an alternative to $\epsilon_{nn'}$. This mixing angle serves to diagonalize the Hamiltonian of equation 4 when $\left|\vec{B}\right| = 0$. As above, due to the non-observation of anomalous loss mechanisms in material

[1] In addition to the “neutron lifetime anomaly” between “beam” and “bottle” experiments, a second 3σ anomaly exists between experiments storing UCN in material bottles ($\tau_n = 880.0 \pm 0.7$ s) [23, 25], and storing UCN in magnetic bottles ($\tau_n = 877.8 \pm 0.2$ s) [24, 27]. The introduction of a transition magnetic moment η_B could potentially resolve this second discrepancy.

traps, θ_0 is limited to $< 10^{-3}$. In the presence of a nonzero magnetic field $\vec{B}$, the angle required for diagonalization of the Hamiltonian, θ_B, will be:

$$\tan 2\theta_B = \frac{2\epsilon_{nn'}}{\Delta m \pm |\mu_n B|} = \frac{\tan 2\theta_0}{1 \pm |\mu_n B| / \Delta m}, \quad (6)$$

where the $\pm$ indicates the possible presence of two polarizations of the neutron. For an unpolarized beam of neutrons, half of the neutrons can reach the resonant condition $\Delta m = \mp |\mu_n B|$.

When the transition angle approaches its maximum, at $\theta_B \to 45°$, the transition probability will be determined by $\epsilon_{nn'}$, the neutron velocity v, and the gradient of the magnetic field B. This is a classical case of the Landau-Zener (LZ) non-adiabatic level-crossing transition, as seen in solar neutrinos [34], which enhances the transformation $n \to n'$. In the case of a beam of n passing through a magnetic field where $\Delta_m < |\mu_B B|$, these LZ transitions occur twice; one "level crossing" occurs at the entrance of the field and one "level crossing" occurs at the exit of the field. If the beam of neutrons is unpolarized, the polarity of the magnetic field does not matter as half of the neutrons will still undergo a LZ transition. The amplitude of these transitions will depend on the initial phase of the oscillating (n, n') system and the velocity of the neutron as it passes through the "level crossing."

Calculation of the overall oscillation probability requires solving the Liouville von Neumann density matrix equation [31, 35]:

$$\frac{d\hat{\rho}}{dt} = -i\hat{\mathcal{H}}\hat{\rho} + i\hat{\rho}\hat{\mathcal{H}}^\dagger = -i\left[\mathcal{H}_{\text{osc}}, \hat{\rho}\right] - i\left\{\mathcal{H}_{\text{int}}, \hat{\rho}\right\} \quad (7)$$

where $\hat{\rho} = |\Psi(t)\rangle \langle\Psi(t)|$ is a 4×4 Hermitian density matrix. This matrix $\hat{\rho}$ can be expressed as the product $\rho_{i,j} = \psi_i(t)\psi_j^\star(t)$ of the wavefunctions for i, j representing polarities of n, n'. In particular, the diagonals of these matrices $\rho_{11}(t)$ and $\rho_{22}(t)$ respresent the probability of being found in either a pure n or n' state, respectively. The density matrix is Hermitian such that the off-diagonals satisfy $\rho_{12}^\star = \rho_{21}$.

Inside absorbing matter with a potential $V - iW$, oscillations between the neutron and mirror neutron states continue. This contributes to an attenuation of $\rho_{22}(t)$, the probability of being a pure n' across an absorber [31]. This attenuation leads to a "void region" of reduced sensitivity when a magnetic field exactly compensates for V.

Frank: Figure with impact of absorber choice.

Yuri: More on impact of absorber, in context of STEREO.

Cary: Comment on how STEREO does their limits?

Experimental Landscape

The existence of mirror matter would cause observable consequences, which would be measurable in the laboratory. Astrophysical constraints on (n, n') mixing come from mass losses in pulsars and temperatures of neutron stars [36–38]. Experimental limits on the Mirror Model rely upon specific assumptions about the nature of Δm and $\vec{B}'$. The most stringent transition limits, $\tau_{nn'} > 448$ s (90% C.L.) come from the perfectly degenerate case, with identical mass splittings and no $\vec{B}'$ [39]. In such a ultracold neutron (UCN) storage experiment, the loss rate of neutrons inside of a container is measured as a function of the local magnetic field. The storage time would be measured at $\left|\vec{B}\right| \ll 10$ nT and for the $\left|\vec{B}\right| > 1\mu$ T. In a perfectly degenerate case, $\Delta m = 0$ with no $\vec{B}'$, the magnetic field thus suppresses the rate of oscillation and limits the transition probability.

In the case where a mirror magnetic field exists or there is a non-zero Δm, the $\left|\vec{B}\right| \ll 10$ nT state would not induce the maximum frequency of oscillations. The presence of a mirror magnetic field $\vec{B}'$ can be probed by utilizing an equal strength magnetic field in two directions, $B_\uparrow$ and $B_\downarrow$, and measuring the asymmetry $A_{\uparrow\downarrow}$ in stored UCN [40]:

$$A_{\uparrow\downarrow} = \frac{n(B_\uparrow) - n(B_\downarrow)}{n(B_\uparrow) + n(B_\downarrow)} \quad (8)$$

This asymmetry can be measured for different field strengths and directions to search directly for $\vec{B}'$. An additional asymmetry E_0 can be produced with the zero field case:

$$E_0 = \frac{2n(B = 0)}{n(B_\uparrow) + n(B_\downarrow)} - 1 \quad (9)$$

Re-analyses of previous experiments have reported a result consistent with $n \to n'$ losses for nonzero $\vec{B}'$ [41, 42]. Subsequent searches for $n \to n'$ have utilized repurposed experiments to search for the neutron electric dipole moment which have excluded most of these claimed signals [43–46]. In addition to using UCN storage, further $n \to n'$ disappearance searches at higher energies have been proposed using beams of UCN passing through a guide with a tunable magnetic field [47].

Neutron regeneration experiments search for the double transition $n \to n' \to n$ [48, 49]. Neutrons shot at an absorber would be regenerated on the other side, in parallel with similar experiments using photons through a wall to search for exotic electromagnetic couplings [50]. In searches for a sterile neutron n' going to a separate brane, experiments use the Fermi potential V of materials to compensate the energy splitting between the n and n' state. Explicit searches for this coupling have been probed, placing strong limits on a completely sterile n' [51, 52]. Further searches for this mechanism have been proposed [53]. In this alternate brane formulation of the sterile neutron, n' has no interaction with the matter through which it passes. This differs with the mirror model formulation described in the previous section, where the n' state attenuates in normal matter, leading to a reduction in transmission.

Cary: More background on STEREO and MUR-MUR

Neutron-mirror neutron mixing has been invoked as an explanation for the neutron lifetime discrepancy [19]. This would manifest itself in a potentially higher mass splitting Δm than probed in the small $\vec{B}'$ search experiments. An experimental probe of this effect was proposed at Oak Ridge National Laboratory (ORNL), utilizing the Spallation Neutron Source (SNS) and the High Flux Isotope Reactor (HFIR) [54, 55]. Initial results from this sequence have excluded $n \rightarrow n'$ transitions as an explanation for the neutron lifetime discrepancy [56][2] We improve upon the results of our previous experiment in reference [56] to further limit the observed amount of neutron-mirror neutron mixing.

EXPERIMENTAL APPARATUS

The measurement reported here was performed at the Spallation Neutron Source (SNS) at Oak Ridge National Laboratory using the Magnetism Reflectometer (MagRef) instrument [57, 58], including some improvements over the previous search reported in [56]. A diagram of the MagRef beamline configuration in this experiment can be seen in Figure 3. The SNS produces H- ions which are accelerated by the linear accelerator to 1 GeV and a nominal power of 1.4 MW (to be increased to 2 MW as part of a planned upgrade). The accelerated H- beam is stripped of electrons by a diamond foil, and then collected and intensified in the accumulator ring, then the protons are extracted in 700 ns long bunches with a repetition rate of 60 Hz which bombard a liquid mercury target to produce fast neutrons by spallation. The charge in each proton bunch is measured by an integrating current beam monitor with an accuracy of 3% [59].

The neutrons viewed by the MagRef beamline are moderated by a 20 K liquid hydrogen moderator. Cold neutrons are emitted with a time scale of tens of μs. The neutrons are transported by a curved beamguide to the experimental area which has a broadening effect on the arrival time, especially of longer wavelength neutrons.

[2] The introduction of η_B in equation 2 has not been probed by this experimental sequence. This exclusion limit assumes that there is not a transition magnetic moment.

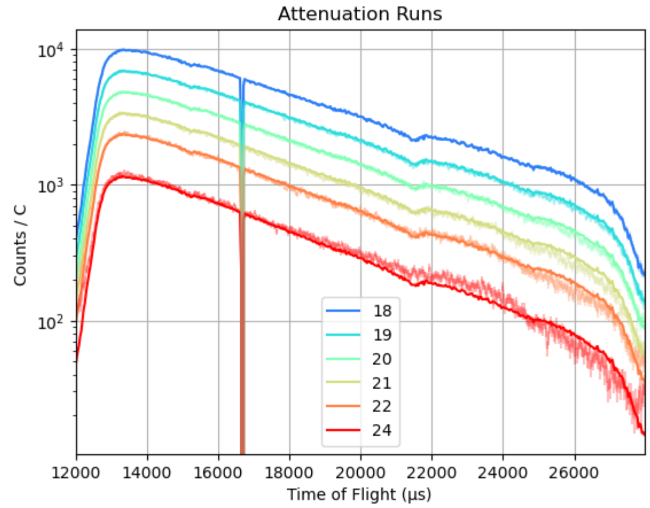

FIG. 1. Fitted time of flight spectrum for neutrons hitting the MagRef detector during attenuation runs. This includes a 50 μs cut at 16666 μs to exclude fast neutrons.

The time of flight (TOF) of neutrons is recorded as the difference between the arrival time at the MagRef detector and the 60 Hz pulse of the accelerator. A system of beam choppers selected a neutron wavelength interval of 2.2 to 5.1 Å. The TOF spectrum of neutrons is shown in Figure 1. The TOF can be related to the neutron wavelength using the length of the beam path and calibrated using observed dips in the TOF spectrum caused by Bragg scattering of neutrons from aluminum at 4.05 and 4.68 Å.

Matt: (Or a beamline scientist?) TOF to wavelength/velocity calibration.

On exiting the beamguide inside the biological shielding surrounding the target monolith, the neutrons encounter a set of vertical and horizontal B_4C blades serving as an aperture which allows a neutron beam with a maximum permitted extent of 30 mm×30 mm to enter the MagRef experimental area. The neutrons travel unimpeded through air approximately 2 m before encountering a second aperture which defines the divergence of the beam. The aperture settings were optimized to maximize the intensity through the beam-catcher (see section on intensity below) without any loss or scattering of neutrons through the beam-catcher walls. The upstream collimator permitted a beam extent of $10\times10\,\mathrm{mm}^2$ and the downstream collimator permitted a beam extent of $8\times6\,\mathrm{mm}^2$ (horizontal × vertical). Although MagRef has the capability to polarize the neutron beam, the beam was not polarized in these measurements.

Matt: Neutron Camera studies + Beam Profile?

The MagRef detector is read out with an array of 304×256 $(X \times Y)$ pixels, each with size 0.7×0.7 mm^2.

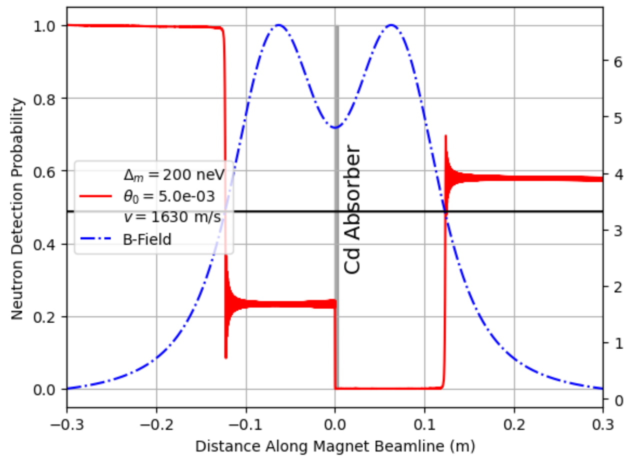

FIG. 2. Transmission of a single neutron through the Cd absorber inside the maximum magnetic field. Description in text. (Color online)

Frank: Request by Leah to do trajectories (1) over the magnetic field (2) right at the "void region" for B_4C. Request by Matt to show many different velocities with same $\Delta m, \theta_0$.

For this measurement, this detector was positioned perpendicular to the beam axis. The maximum counting rate of the detector is limited by the output electronics, which lead to a dead time of 4 μs. Each detected neutron is subsequently recorded into a DAQ system which includes a GPS-based time tag, the (X, Y) position of the pixel in the detector, the time-of-flight, and the proton charge for the SNS pulse that produced the neutron. The detector was surrounded by improved shielding, further reducing the backgrounds.

The MagRef beamline uses a double-solenoid magnet that has a characteristic double-peaked behavior [60]. The peak field in the center of either of these two solenoids is 6.6 T, while the peak field at the center of the apparatus is 5 T. A field profile with the trajectory of a neutron can be seen in figure 2. The oscillation probability of the (n, n') state depends on the magnetic field and the orientation of the neutron spin. The search was conducted with the center of the magnetic field set to ± 4.7 T and ± 2.35 T, as well as a background measurement with no magnetic field. The beam is unpolarized, and so the oscillation probability should be independent of the polarity of the magnetic field.

Leah: Alignment? Field Mapping? I have a comment that this is a different magnetic field so reference [60] is wrong.

Frank: Magnet stability figure(?) or calculation

The experiment relies upon a double transition $n \rightarrow n'$ on one side of an absorber, and a subsequent transition $n' \rightarrow n$ on the other side. A general diagram of the experimental setup can be found in figure 3, which is similar to that of our previous work in [56]. Inside of the magnet, we place an absorber to remove neutrons while allowing n' transmission. We have changed the neutron absorber used in the beam path from 32 mm of B_4C as used previously to 3.5 mm of Cadmium (Cd). The Fermi potential V of B_4C is 199.2 neV, while that of Cd is 58.8 neV [31]. This switch moves the region of low sensitivity immediately around the Fermi potential inside the peak of the magnetic field. As a result, the void region present in our apparatus is suppressed by the magnetic field and has already been excluded by previous results.

Leah: Uncertainty of positioning absorber and apertures

In addition to data taken with the beamstopper in place, we used a series of runs without the beamstopper and the magnet turned off to determine the intensity of the neutron beam. We used a set of commercial plates of polycarbonate (PC) $(C_{16}O_3H_{14})_n$ with thickness 1.27 mm. Beam attenuation in the PC is mostly due to elastic scattering on hydrogen, so together with attenuation of non-scattered beam and small absorption, a small amount of scattering background was generated. TOF dependence of absorption will be discussed further down in section on intensity. There were some studies using a pinhole to heavily collimate the beam. These studies of attenuation did not have the magnetic field turned on, thus had a nominal field of 0 T, with no absorber in place.

RESULTS

Intensity

The SNS produces too many neutrons to directly measure with our detector, and so we must use indirect methods. The beam profile can be seen in figure 4. The direct beam-on area is used to determine a Region of Interest (ROI) for the signal region. Outside of our ROI, there is a background due to neutron scatter in the absorbers or other elements of the upstream beamline. This background was directly measured in the regions adjacent to the unscattered beam and then subtractred from the seen counts in the ROI. The shape of the subtracted background was observed to be consistent with the shape of the background observed in the detector. Wavelength spectrum of these neutrons was reconstruced by using a special run with a 0.2 mm pinhole installed 2.5 m upstream of the neutron detector.

Matt: Discussion of pinhole data

We determine the expected intensity in our detector by looking at data taken with polycarbonate blocks in the beamline, which serves to attenuate the beam. The neu-

FIG. 3. Diagram of the MagRef beamline with the Cd absorber in place.

Leah: Remake this figure with Cadmium/changed slits(?)

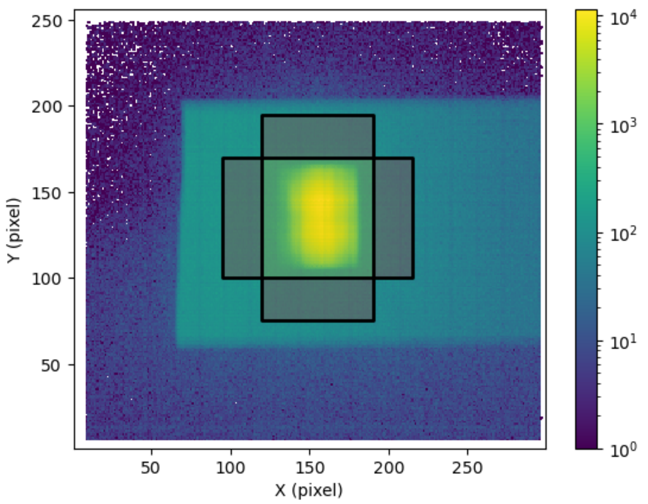

FIG. 4. The sum of all 6 runs with PC boards in place and no Cd beam stop in place. The neutron beam can be clearly seen centered around pixels $(X, Y) = (170, 135)$. Shielding around the detector causes a sharp falloff in the background above $Y = 200$ and below $Y = 70$, as well as the left side of the detector around $X \sim 75$. The region of interest is highlighted in the center, with the signal area surrounding the beam and the background area chosen to fit inside the less shielded region.

Frank: Do this plot with just 18 PCs

tron counts per Coulomb was measured with as few as 18 and as many as 24 polycarbonate blocks. Fewer than 18 blocks, and the associated higher intensity, would potentially damage the detector and activate parts of the beamline. Actual production data with the Cadmium absorber in place was taken with zero polycarbonate blocks in the beamline. The uncertainties in this intensity come predominately from the method of extrapolation.

The intensity of the unimpeded beam, I_0, can be described by an arbitrary function:

$$I_0 = f(I(N); N). \tag{10}$$

Here we use the measured intensity I as a function of the number of polycarbonate blocks inserted into the beam N to determine I_0. As a first approximation, the intensity function is polynomial, such that $I_0 = I(N)\eta^{-N}$, where we define an attenuation factor η. We can then measure $I(N)$ in our ROI, and use these measured values to fit for $\eta = XXX$. The function 10 can then be extrapolated back to $N = 0$ to find the number of neutrons we expect to see on the detector This determination gives us a value of $I_0 = YYY$. neutrons/C.

Frank: Flat Intensity η and I_0

A more accurate determination of the intensity uses the fact that the polycarbonate block has a velocity dependent attenuation $\eta(v)$. In the case that the cross section of our polycarbonate depends on neutron velocity v as $1/v$, we can expand the attenuation factor η in terms of the time of flight t:

$$\eta(t) = \eta_0 + \eta_1 t \tag{11}$$

We can then use modified attenuation factor to map the intensity I to a function:

$$I(N, t) = (\eta_0 + \eta_1 t)^N, \tag{12}$$

A linear regression can be used to fit these parameters, such that $\eta_0 = 0.7554(6)$ and $\eta_1 = -0.424(3)$. This can be extrapolated back to $N = 0$ to get a total intensity of $(2.95 \pm 0.10) \times 10^9$ neutrons/C. The increase in intensity and reduction in uncertainty over the previous measured value of $(1.05 \pm 0.31) \times 10^9$ comes from improvements in positioning the slits so that we are not scattering as much of the beam. These uncertainties are dominated by the fitting procedure. Additional uncertainties come from the orientation and thickness of the PC plates.

Matt: Discussion of uncertainties due to PC plates

These results have been validated through comparison with a Particle and Heavy Ion Transport System (PHITS) simulation of the beamline [61]. This allows us to look for deviations from exponential behavior in the extrapolation method.

Lawrence: Discussion of intensity simulations. (Coordinate with Devyn?)

Search for Effect

The transition probability for $n \to n' \to n$ was probed with variable magnetic field with the Cd absorber in place. The presence of oscillations into the mirror neutron state and back depends on the energy splitting between the two states. By adjusting the magnetic field, this transition probability is enhanced. An example signal seen in the detector with an absorber in place, formed by combining the runs taken with 0 T, can be seen in figure . The probability of transition can be extracted by looking for a signal appearing over a background. Since the transition probability depends on magnetic field, the background can be found when $B = 0$ T, and then compared to the signal seen in the same region when $B = \pm 4.7$ T or $B = \pm 2.35$ T.

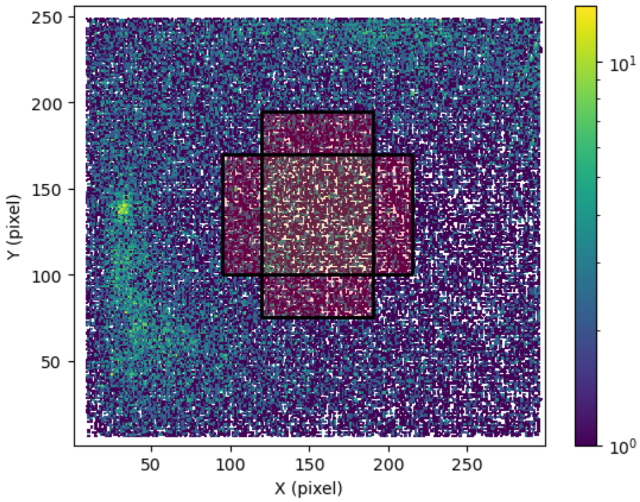

FIG. 5. The sum of all 19 runs taken with the magnetic field off and the cadmium absorber in place. The signal region of interest is highlighted in orange in the center, while the regions used for extraction of backgrounds are highlighted in red on the sides of the signal region of interest.

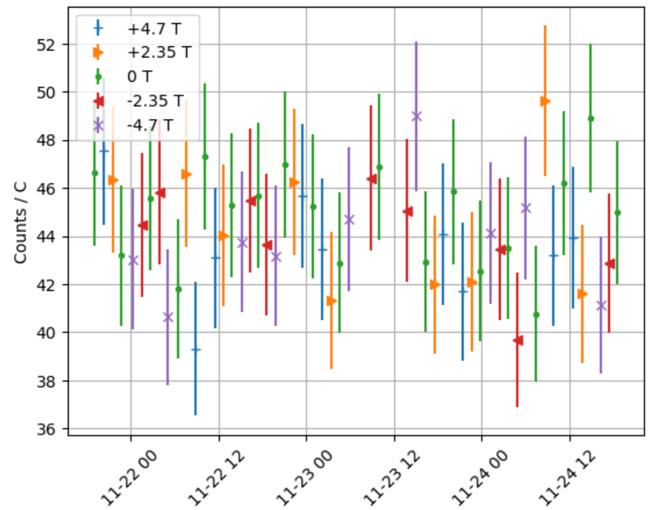

FIG. 6. Measured neutron counts / C inside the region on interest for each run. Runs are categorized by nominal magnetic field. (Color online)

The signal passing through the absorber was investigated by counting neutron events appearing in the detector inside of a square 70 by 70 pixel region of interest. This region was chosen to incorporate the beam profile seen with various intensity runs as seen in Figure 4. The SNS runs at 60 Hz, which induces a periodic background due to fast neutrons every 16666 μs. To avoid this background, we place a veto with width 55 μs on events with a time of flight between 16661 μs and 16711 μs. Data was collected in a constant charge mode, such that the integrated charge on the accelerator target for a given run was 5.1 C. This meant that temporary outages of the accelerator took longer to run, leading to suppressed rates during these outages. Accelerator pulses in the analysis chain are associated with the charge of the proton pulse deposited. Accelerator pulses where less than 23 μC are deposited into the target are removed from the analysis.

Frank: Accelerator stability figure

With these cuts, the signal can be measured for each individual run and normalized to the accumulated charge for that run. Counts inside the region of interest for individual runs can be seen in figure 6. Uncertainties on the counts inside the region of interest assumed a Gaussian distribution, and the error bars indicate one standard deviation. These can then be combined to provide an overall signal for different magnetic fields, as can be seen in table I.

The probability of neutrons undergoing the transition $n \rightarrow n'$ should be dependent on the energy difference between the two states. As a systematic check, the region around the region of interest can be used to determine the expected background for a given magnetic field, as in table II. A background region can be formed, extending 25 pixels on each side of the square region of interest, to determine the background expected during each run. The backgrounds determined from all four sides of the region of interest overestimates the signal seen in the foreground region, as the detector sits in a saddle point in the vertical (Y) direction. The effect of this saddle point can be mitigated by using only the background regions in the horizontal plane of the detector, on the left and right of the signal. The background rate estimated for each run using this method can be seen in figure 7. The number of counts seen in the foreground region, where we would see $n \rightarrow n' \rightarrow n$ transitions, is consistently lower than the estimate of counts outside this region. As a result, the most conservative determination of the transition rate uses the comparison of $B \neq 0$ T runs with $B = 0$ T runs.

The nominal background could be sensitive to other effects, which could induce a time dependence or additional position dependence in the backgrounds. The sensitivities of backgrounds to various systematics was investigated.

Leah: Systematics due to time-dependence in backgrounds?

This served to inflate the uncertainty due to the signal by [XXX]. Discuss more analysis on backgrounds, background studies and reduction, TOF spectrum, time dependence, position dependence, prompt backgrounds. Do we have a systematic uncertainty to add?

B Field (T)	Live Time (s)	Foreground Counts	Total Charge (C)	Counts / C
+4.7	33147	1987 ± 46	45.6	43.5 ± 1.0
+2.35	32726	2027 ± 45	45.6	44.4 ± 1.0
0	81179	4324 ± 66	96.3	44.9 ± 0.7
−2.35	32801	2010 ± 45	45.6	44.1 ± 1.0
−4.7	39014	1999 ± 44.7	45.6	43.9 ± 1.0

TABLE I. Combined signal in foreground region for each magnetic field foreground signal for each magnetic field. Uncertainties are statistical and represent one statistical deviation.

B Field (T)	Background Counts	Flat Background / C	Horizontal Background / C
+4.7	3292 ± 57.4	51.2 ± 0.9	45.7 ± 1.2
+2.35	3313 ± 57.6	51.6 ± 0.9	47.5 ± 1.3
0	7100 ± 84	52.3 ± 0.6	47.9 ± 0.9
−2.35	3387 ± 58	52.8 ± 0.9	47.9 ± 1.3
−4.7	3406 ± 58	53.0 ± 0.9	47.0 ± 1.3

TABLE II. Calculated background signal for each magnetic field. Raw background counts have statistical uncertainties of one standard deviation. The Flat Background / C and Horizontal Background / C columns have been extrapolated across the region of interest for direct comparison with foreground counts.

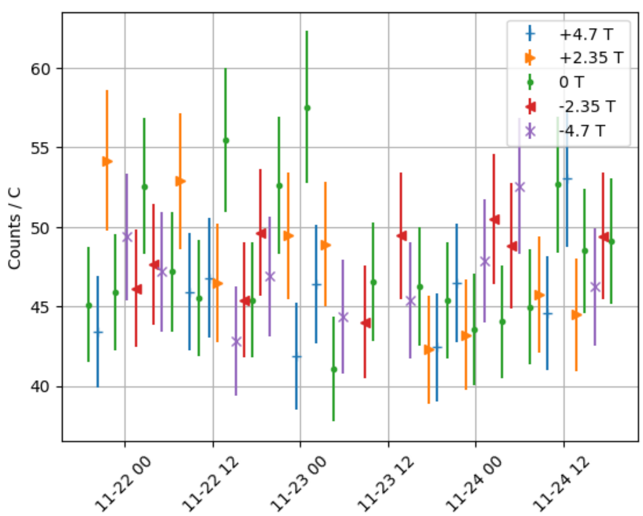

FIG. 7. Background counts / C expected in the foreground region of interest, determined by using only the horizontal (left and right) background regions. Runs are categorized by nominal magnetic field. (color online)

Simulations of Neutrons in Matter and Magnetic Fields

The probability of $n \to n'$ transmission through the absorber can be calculated for varying Δm and θ_0 parameters, as defined in equation 6 [19]. The time-evolution of the density matrix following equation 7 with the Hamiltonian of equation 4 can then be solved numerically. These utilize a custom GPU simulation package in the Julia programming language. The Liouville-von Neumann equation, equation 7, can be written using in the matrix form $\dot{\rho} = \mathbf{M}\rho$, where within a small step dz the matrix $\mathbf{M}$ is constant. The solution to the differential equation can be found with the matrix exponential:

$$\rho\,(t) = e^{\mathbf{M}t}\rho_0 \tag{13}$$

The matrix exponential is calculated by finding the Jordan decomposition of the matrix $\mathbf{M}$:

$$\mathbf{M} = SJS^{-1} \qquad e^{\mathbf{M}t} = Se^{Jt}S^{-1} \tag{14}$$

Since the density matrix $\hat{\rho}$ of the Liouville-von Neumann equation, equation 7, is Hermetian, the equation can be rewritten in the form:

$$\begin{pmatrix} \dot{\rho}_{11} \\ \dot{a} \\ \dot{b} \\ \dot{\rho}_{22} \end{pmatrix} = \frac{1}{\hbar} \begin{pmatrix} -2W & 0 & -2\epsilon & 0 \\ 0 & -W & -U & 0 \\ \epsilon & U & -W & -\epsilon \\ 0 & 0 & 2\epsilon & 0 \end{pmatrix} \begin{pmatrix} \rho_{11} \\ a \\ b \\ \rho_{22} \end{pmatrix}. \tag{15}$$

In equation 15, we have used the Hermiticity of $\hat{\rho}$ to relate the off-diagonal components of the density matrix $\rho_{12} = a + ib$ and $\rho_{21} = a - ib$. We can then solve equation 14 numerically for individual neutron trajectories with a fixed Δm, θ_0, and velocity v using the matrix described in equation 15. We begin this calculation with a density matrix at $t = 0$ in the pure neutron state:

$$\hat{\rho} = \begin{pmatrix} \rho_{11} & \rho_{12} \\ \rho_{21} & \rho_{22} \end{pmatrix} = \begin{pmatrix} 1 & 0 \\ 0 & 0 \end{pmatrix}. \tag{16}$$

The potentials in equation 15 come from the presence of magnetic fields and material optical potentials. The magnetic field profile of figure 2 was provided by the manufacturer and converted into a cubic spline for interpolation. This was extended out to a constant field of 50 μT, accounting for the Earth's magnetic field, outside of the profile. As the magnetic field $\vec{B}$ couples to the spin of the neutron $\vec{\mu}_n$, the calculation must be run for each spin $\pm\mu_n$ state separately and subsequently averaged.

Material	$V + iW$ (eV)
Cd	$5.88 \times 10^{-8} + i\left(8.46 \times 10^{-9} + v \cdot 9.91 \times 10^{-15}\right)$
B_4C	$1.99 \times 10^{-7} + i\left(6.10 \times 10^{-9} + v \cdot 2.40 \times 10^{-14}\right)$
Air	$5.67 \times 10^{-11} + i\left(5.77 \times 10^{-15} + v \cdot 8.33 \times 10^{-18}\right)$

TABLE III. Material optical potentials used for calculating probability of neutron transmission through an absorber [31].

Centered inside the magnetic field is a highly absorbing Cd beamstop with thickness 3.5 mm. In the 2019 dataset previously reported, we utilized a 32 mm thick B_4C beamstop instead [56]. In addition to the optical potential of the absorber, the experimental apparatus was placed in air at room temperature, which has an additional optical potential. We simulated these materials with both real and imaginary parts of the material optical potentials, using values in table III. These were simulated with one edge of the material absorber sitting at the midpoint of the magnetic field. The addition of air instead of vacuum outside of the absorber provides a ~ 1 % reduction in sensitivity for a given neutron trajectory.

The imaginary part of the optical potential, W, couples to the velocity of the neutrons passing through the material. Each velocity has a distinct probability of transitioning in the Landau-Zener non-adiabatic condition. The velocity dependence was accounted for by averaging across 2000 trajectories with fixed velocity, sampled from the velocity profile of neutrons coming from the SNS. This is numerically integrated with steps of constant $z = 10$ μm. The simulated probability for a given neutron trajectory has a characteristic oscillation due to the finite steps with a fixed velocity v. To mitigate any uncertainties due this oscillation, the probability of transmission is averaged over the final 1 mm (100 steps). An alternate form of accounting for velocities utilizes an averaging of initial phases. This method is less computationally expensive, but faces numerical precision complications at material interfaces.

Yuri: More about the initial phase averaging method vs. averaging over velocities

The results of the simulation described above for a Cd absorber with the two nominal magnetic fields, 4.7 T and 2.35 T, can be seen in figure 8. The highest sensitivity to $n \to n'$ oscillations can be found near the magnetic field peak. A reduced sensitivity can be seen for high θ_0 values near the optical potential of Cd. For values of $\Delta m > \mu_n \cdot B_{max}$, the sensitivity of the experiment tends to a constant value. At low mass splitting, characterization of the magnetic field becomes more dependent on the field profile, and ultimately tends towards the zero-field case.

Frank: Limits extrapolated to $\Delta m \to 0$? Any comment on negative Δm

Leah: More detail about the different studies we did to rule out e.g. numerical precision errors, bin size errors? Something about experimental errors like positioning of equipment inside magnet.

Limits

Determination of the limit on $n \to n' \to n$ utilizes the Feldman-Cousins method for treatment of rare events [62]. The Feldman-Cousins band chooses a band of likelihoods based on finding the closest likelihood values to the maximum likelihood. This can then be used to determine the 95 % confidence limit. Here we assumed Gaussian uncertainties for the signal and backgrounds. In the event of a systematic bias in the expected intensity, the reported 95 % C.L limit on transmission $p_{tr.}$ is underestimated.

B-Field (T)	Signal ($\times 10^{-10}$ n/C)	95 % C.L. $p_{tr.}$ ($\times 10^{-10}$)
±4.7	-4.26 ± 3.41	3.27
±2.35	-2.35 ± 3.42	4.52
0	-10.87 ± 3.98	1.86

TABLE IV. Neutron transmission through the Cd absorber for varied magnetic fields. The ±4.7 T and ±2.35 T datasets use both polarities with the 0 T data taken as a background. The 0 T dataset uses the background region of interest to estimate the background in the beam

The intensity of $(2.95 \pm 0.10) \times 10^9$ neutrons / C can be compared with the signal measured at various magnetic fields in tables I and II. We use the 0 T data inside the ROI as a background measurement. The beam is unpolarized and so the $+4.7$ T result can be combined with the -4.7 T results, and the same can be done for the ±2.35 T datasets. The counts measured in the 0 T field runs are greater than any single other magnetic field profile, leading to a significant improvement between this result and the previous due to statistical fluctuation.

The overall parameter space excluded by this experiment can be found by taking the 95 % C.L. $p_{tr.}$ and superimposing this on the simulated regions of exclusion for the respective magnetic fields. The ±4.7 T and ±2.35 T results can further be combined by taking a weighted average of the two exclusion limits. The results can be seen in figure . As $\Delta_m \to \infty$, we see the probability begin to level off. Our highest sensitivities are at the peak field strengths of our magnet, with additional sensitivity near the flat region between the two peaks.

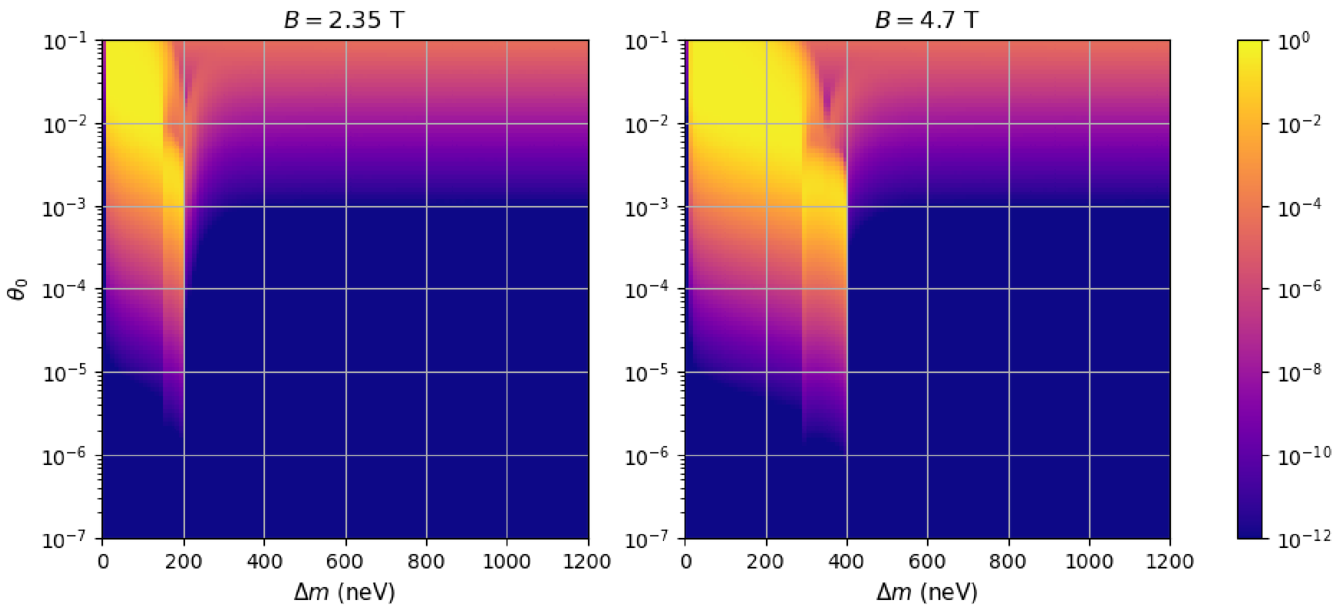

FIG. 8. Simulated probability of transmission through 3.5 mm of Cadmium in a 2.35 T (left) peak strength magnetic field and 4.7 T (right) peak strength.

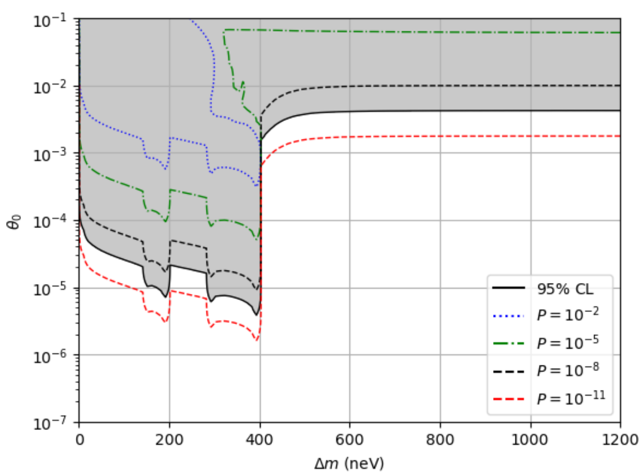

FIG. 9. Limits reported in this paper.

Frank: Remake figure to include previous paper's limits and compare with STEREO, nEDM, Saenz-Arevalo

CONCLUSIONS

We have reported on an experiment that provides the most stringent results for $n \to n'$ oscillations in the region around $50 \leq |\Delta E| < 400$ neV. Unlike results presented in reactor experiments, the regeneration technique using unpolarized neutrons is relatively insensitive to the sign of the ΔE. This technique can also be used at higher intensity neutron sources, such as ORNL's High Flux Isotope Reactor (HFIR), with limiting systematics due to knowledge of the intensity. This limit is competitive even with sterile neutron searches that reject any intrinsic interaction between n' and matter. This result is the next step in a suite of experiments planned at ORNL to probe $\not{\mathcal{B}}$ violation.

Cary: Any reduction in limits from STEREO / MURMUR?

ACKNOWLEDGEMENTS

This research was sponsored by the U.S. Department of Energy (DOE), Office of Science, Office of Nuclear Physics [contract DE-AC05-00OR22725], by the Laboratory Directed Research and Development Program [project 8215] of Oak Ridge National Laboratory, managed by UT-Battelle, LLC, for the U. S. DOE, and in part by the U.S. DOE, Office of Science, Office of Workforce Development for Teachers and Scientists (WDTS) under the Science Undergraduate Laboratory Internship program. This research used resources at the Spallation Neutron Source, a DOE Office of Science User Facility operated by the Oak Ridge National Laboratory.

[1] M. Battaglieri *et al.*, in *U.S. Cosmic Visions: New Ideas in Dark Matter* (2017) arXiv:1707.04591 [hep-ph].

[2] K. K. Boddy, M. Lisanti, S. D. McDermott, N. L. Rodd, C. Weniger, Y. Ali-Haïmoud, M. Buschmann, I. Cholis,

D. Croon, A. L. Erickcek, *et al.*, Journal of High Energy Astrophysics **35**, 112 (2022), arXiv:2203.06380.

[3] S. Tulin and H.-B. Yu, Physics Reports **730**, 1 (2018), arXiv:1705.02358.

[4] S. Adhikari, A. Banerjee, K. K. Boddy, F.-Y. Cyr-Racine, H. Desmond, C. Dvorkin, B. Jain, F. Kahlhoefer, M. Kaplinghat, A. Nierenberg, *et al.*, , 1 (2022), arXiv:2207.10638.

[5] F.-Y. Cyr-Racine and K. Sigurdson, Physical Review D **87**, 103515 (2013), arXiv:1209.5752.

[6] T. D. Lee and C. N. Yang, Physical Review **106**, 254 (1957).

[7] I. Y. Kobzarev, L. B. Okun, and I. Y. Pomeranchuk, Sov. J. Nucl. Phys. **3**, 837 (1966).

[8] Z. G. Berezhiani and L. Bento, Physical Review Letters **96**, 081801 (2006), arXiv:0507031 [hep-ph].

[9] Z. Berezhiani, P. Ciarcelluti, D. Comelli, and F. L. Villante, International Journal of Modern Physics D **14**, 107 (2005), arXiv:0312605 [astro-ph].

[10] A. Coc, M. Pospelov, J.-P. Uzan, and E. Vangioni, Physical Review D - Particles, Fields, Gravitation and Cosmology **90**, 1 (2014), arXiv:1405.1718.

[11] F.-Y. Cyr-Racine, F. Ge, and L. Knox, Physical Review Letters **128**, 201301 (2022), arXiv:2107.13000.

[12] Z. Berezhiani, P. Ciarcelluti, S. Cassisi, and A. Pietrinferni, Astroparticle Physics **24**, 495 (2006), arXiv:0507153 [astro-ph].

[13] R. Ciancarella, F. Pannarale, A. Addazi, and A. Marcianò, Physics of the Dark Universe **32**, 100796 (2021), arXiv:2010.12904.

[14] A. Howe, J. Setford, D. Curtin, and C. D. Matzner, Journal of High Energy Physics **2022**, 59 (2021), arXiv:2112.05766.

[15] $|\Delta\mathcal{B}| = 2$*: A State of the Field, and Looking Forward–A brief status report of theoretical and experimental physics opportunities* (2020) arXiv:2010.02299 [hep-ph].

[16] A. Addazi *et al.*, J. Phys. G **48**, 070501 (2021), arXiv:2006.04907 [physics.ins-det].

[17] Z. G. Berezhiani, The European Physical Journal C **81**, 33 (2021), arXiv:2002.05609.

[18] M. Sarrazin, G. Pignol, J. Lamblin, F. Petit, G. Terwagne, and V. V. Nesvizhevsky, Physical Review D **91**, 075013 (2015), arXiv:1501.06468.

[19] Z. Berezhiani, European Physical Journal C **79** (2019), 10.1140/epjc/s10052-019-6995-x, arXiv:1807.07906.

[20] A. Serebrov, V. Varlamov, A. Kharitonov, A. K. Fomin, Y. Pokotilovski, P. Geltenbort, J. Butterworth, I. A. Krasnoschekova, M. S. Lasakov, R. Tal'daev, *et al.*, Physics Letters, Section B: Nuclear, Elementary Particle and High-Energy Physics **605**, 72 (2005).

[21] A. Pichlmaier, V. Varlamov, K. Schreckenbach, and P. Geltenbort, Physics Letters B **693**, 221 (2010).

[22] A. Steyerl, J. M. Pendlebury, C. Kaufman, S. S. Malik, and A. M. Desai, Physical Review C - Nuclear Physics **85**, 1 (2012).

[23] S. Arzumanov, L. Bondarenko, S. Chernyavsky, P. Geltenbort, V. Morozov, V. Nesvizhevsky, Y. Panin, and A. Strepetov, Physics Letters B **745**, 79 (2015).

[24] V. F. Ezhov, A. Z. Andreev, G. Ban, B. A. Bazarov, P. Geltenbort, A. G. Glushkov, V. A. Knyazkov, N. A. Kovrizhnykh, G. B. Krygin, O. Naviliat-Cuncic, and V. L. Ryabov, JETP Letters **107**, 671 (2018), arXiv:1412.7434.

[25] A. P. Serebrov, E. A. Kolomensky, A. K. Fomin, I. A. Krasnoschekova, A. V. Vassiljev, D. M. Prudnikov, I. V. Shoka, A. V. Chechkin, M. E. Chaikovskiy, V. E. Varlamov, *et al.*, Physical Review C **97**, 055503 (2018), arXiv:1712.05663.

[26] R. W. Pattie *et al.* (UCNτ), Science **360**, 627 (2018), arXiv:1707.01817.

[27] F. Gonzalez *et al.* (UCNτ), Physical Review Letters **127**, 162501 (2021), arXiv:2106.10375.

[28] J. S. Nico, M. S. Dewey, D. M. Gilliam, F. Wietfeldt, X. Fei, W. M. Snow, G. L. Greene, J. Pauwels, R. Eykens, A. Lamberty, *et al.*, Physical Review C - Nuclear Physics **71**, 55502 (2005), arXiv:0411041 [nucl-ex].

[29] A. T. Yue, M. S. Dewey, D. M. Gilliam, G. L. Greene, A. B. Laptev, J. S. Nico, W. M. Snow, and F. Wietfeldt, Physical Review Letters **111**, 222501 (2013), arXiv:1309.2623.

[30] N. Sumi, K. Hirota, G. Ichikawa, T. Ino, Y. Iwashita, S. Kajiwara, Y. Kato, M. Kitaguchi, K. Mishima, K. Morikawa, *et al.*, in *Proceedings of the 3rd J-PARC Symposium (J-PARC2019)* (Journal of the Physical Society of Japan, 2021) arXiv:2102.09758.

[31] Y. Kamyshkov, J. Ternullo, L. Varriano, and Z. Berezhiani, Symmetry **14**, 230 (2022), arXiv:2111.01791.

[32] Z. G. Berezhiani, R. Biondi, Y. Kamyshkov, and L. Varriano, Physics **1**, 271 (2019), arXiv:1812.11141.

[33] A. Y. Ignatiev and R. R. Volkas, Physical Review D **68** (2003), 10.1103/PhysRevD.68.023518, arXiv:0304260 [hep-ph].

[34] C. W. Kim, W. K. Sze, and S. Nussinov, Physical Review D **35**, 4014 (1987).

[35] H. Breuer and F. Petruccione, *The Theory of Open Quantum Systems* (Clarendon Press, 2002) p. 110.

[36] I. Goldman, R. N. Mohapatra, and S. Nussinov, Physical Review D **100**, 123021 (2019), arXiv:1901.07077.

[37] D. McKeen, M. Pospelov, and N. Raj, Physical Review Letters **127**, 061805 (2021), arXiv:2105.09951.

[38] I. Goldman, R. N. Mohapatra, S. Nussinov, and Y. Zhang, Physical Review Letters **129**, 061103 (2022).

[39] A. Serebrov, E. B. Aleksandrov, N. Dovator, S. Dmitriev, A. K. Fomin, P. Geltenbort, A. Kharitonov, I. Krasnoschekova, M. Lasakov, A. Murashkin, *et al.*, Nuclear Instruments and Methods in Physics Research Section A: Accelerators, Spectrometers, Detectors and Associated Equipment **611**, 137 (2009), arXiv:0809.4902.

[40] Z. Berezhiani, The European Physical Journal C **64**, 421 (2009), arXiv:0804.2088.

[41] Z. G. Berezhiani and F. Nesti, The European Physical Journal C **72**, 1974 (2012), arXiv:1203.1035.

[42] Z. Berezhiani, R. Biondi, P. Geltenbort, I. A. Krasnoshchekova, V. E. Varlamov, A. V. Vassiljev, and O. M. Zherebtsov, The European Physical Journal C **78**, 717 (2018), arXiv:1712.05761.

[43] I. Altarev, C. A. Baker, G. Ban, K. Bodek, M. Daum, P. Fierlinger, P. Geltenbort, K. Green, M. G. Van Der Grinten, E. Gutsmiedl, *et al.*, Physical Review D - Particles, Fields, Gravitation and Cosmology **80**, 1 (2009), arXiv:0905.4208.

[44] C. Abel *et al.* (nEDM), Physics Letters B **812**, 135993 (2021), arXiv:2009.11046.

[45] N. J. Ayres, Z. G. Berezhiani, R. Biondi, G. Bison, K. Bodek, V. Bondar, P.-J. Chiu, M. Daum, R. T. Dinani, C. B. Doorenbos, *et al.* (nEDM), Symmetry **14**, 503 (2022), arXiv:2111.02794.

[46] P. Mohanmurthy, A. R. Young, J. A. Winger, and G. Zsigmond, Symmetry **14** (2022), 10.3390/sym14030487, arXiv:2201.04191.

[47] W. Saenz-Arevalo, G. Ban, J. Chen, P. J. Chiu, B. Clément, M. Guigue, T. Jenke, P. Larue, T. Lefort, O. Naviliat-Cuncic, *et al.*, in *56th Rencontres de Moriond on Electroweak Interactions and Unified Theories* (2022) pp. 1–4, arXiv:2206.08721.

[48] Z. G. Berezhiani, M. Frost, Y. Kamyshkov, B. Rybolt, and L. Varriano, Physical Review D **96**, 35039 (2017), arXiv:1703.06735.

[49] U. Schmidt, "An Experimental Limit on Neutron Mirror-Neutron Oscillation," (2007).

[50] J. Redondo and A. Ringwald, Contemporary Physics **52**, 211 (2011), arXiv:1011.3741.

[51] C. Stasser, G. Terwagne, J. Lamblin, O. Méplan, G. Pignol, B. Coupé, S. Kalcheva, S. Van Dyck, and M. Sarrazin, The European Physical Journal C **81**, 17 (2021), arXiv:2007.11335.

[52] H. Almazán, L. Bernard, A. Blanchet, A. Bonhomme, C. Buck, P. del Amo Sanchez, I. El Atmani, L. Labit, J. Lamblin, A. Letourneau, *et al.*, Physical Review Letters **128**, 061801 (2022), arXiv:2111.01519.

[53] M. Hostert, D. McKeen, M. Pospelov, and N. Raj, (2022), arXiv:2201.02603 [hep-ph].

[54] L. J. Broussard, K. M. Bailey, W. B. Bailey, J. Barrow, B. Chance, C. B. Crawford, L. Crow, L. Debeer-Schmitt, N. Fomin, M. Frost, *et al.*, in *Proceedings of the 2017 Meeting of the APS Division of Particles and Fields, DPF 2017* (2017) arXiv:1710.00767.

[55] L. Broussard, K. Bailey, W. Bailey, J. Barrow, K. Berry, A. Blose, C. Crawford, L. Debeer-Schmitt, M. Frost, A. Galindo-Uribarri, *et al.*, EPJ Web of Conferences **219**, 07002 (2019).

[56] L. J. Broussard, J. L. Barrow, L. DeBeer-Schmitt, T. Dennis, M. R. Fitzsimmons, M. J. Frost, C. E. Gilbert, F. M. Gonzalez, L. Heilbronn, E. B. Iverson, *et al.*, Physical Review Letters **128** (2022), 10.1103/physrevlett.128.212503, arXiv:2111.05543.

[57] H. Ambaye, R. Goyette, A. Parizzi, and F. Klose, Neutron News **19**, 11 (2008), https://doi.org/10.1080/10448630802210537.

[58] V. Lauter, H. Ambaye, R. Goyette, W.-T. Hal Lee, and A. Parizzi, Physica B: Condensed Matter **404**, 2543 (2009).

[59] W. Blokland, G. Armstrong, C. Deibele, J. Pogge, and V. Gaidash, AIP Conf. Proc. **868**, 238 (2006).

[60] S. Stort, "5 tesla split-pair superconducting magnet system," (2017), accessed: Nov. 22, 2022.

[61] T. Sato *et al.*, J. Nucl. Sci. Tech. **55**, 684 (2018).

[62] G. J. Feldman and R. D. Cousins, Physical Review D **57**, 3873 (1998).